JOURNAL OF AIRCRAFT
Vol. 44, No. 2, March–April 2007

Numerical Simulation of Airfoil Thermal Anti-Ice Operation Part 1: Mathematical Modeling

Guilherme Araújo Lima da Silva,* Otávio de Mattos Silvares,† and
Euryale Jorge Godoy de Jesus Zerbini‡
Escola Politécnica, University of São Paulo, 05508-900 São Paulo, Brazil

DOI: 10.2514/1.544

A mathematical model was developed to both describe an airfoil electrothermal anti-ice system operation and enable prediction of its main parameters. A reference case was chosen to define the mathematical model and support the results validation. The first law of thermodynamics is applied to airfoil solid surface and runback water flow. In addition, liquid water is subjected to mass and momentum conservation principles. The overall heat transfer coefficient, between gaseous flow and airfoil, is very sensitive to solid surface temperature gradients and runback water evaporation, requiring an adequate solution of the thermal boundary layer. Therefore, the mathematical model included dynamic and thermal boundary layer equations in integral form, which considers variable properties, pressure, and temperature gradients on the surface, coupled heat and mass transfer effects, and laminar to turbulent transition region modeling.

Nomenclature

A	=	finite volume area exposed to flow around airfoil, m^2
B_h	=	heat transfer driving force
B_m	=	mass transfer driving force
C_f	=	local friction coefficient $\tau/(1/2 \cdot \rho_e \cdot u_e^2)$
c	=	airfoil chord, m
c_p	=	specific heat, J/(kg · K)
D	=	mass diffusivity, m^2/s
F	=	wetness factor
G	=	mass flux $\rho \cdot u_e$, kg/(s · m^2)
g_m	=	mass transfer conductance, kg/(s · m^2)
h	=	convective heat transfer coefficient, W/(m^2 · K)
i	=	specific enthalpy, J/kg
k	=	thermal conductivity, W/(m · K)
Le	=	Lewis number $c_p \cdot D_{\text{water,air}} \cdot \rho/k$
$l(\lambda)$	=	function of pressure gradient parameter
M	=	Mach number
$\dot{m}$	=	mass flow rate, kg/s
mf_{H2O}	=	water vapor mass fraction in air
Nu	=	gaseous flow local Nusselt number $(h_{\text{air}} \cdot s)/k_{\text{air}} = St_{\text{air}} \cdot Re_s \cdot Pr_{\text{air}}$
Pr	=	Prandtl number $\mu \cdot c_p/k$
p	=	pressure, Pa
p_{mixt}	=	total mixture pressure, Pa
p_{vap}	=	partial vapor pressure, Pa
$\dot{q}''$	=	heat flux, W/m^2
$\dot{q}_{\text{lost}}$	=	heat transfer rate lost to gaseous flow, W
$\dot{\bar{q}}''_{\text{turb}}$	=	mean turbulent heat flux, W/m^2
Re_s	=	Reynolds number based on streamwise distance on airfoil surface $u_e \cdot s/\nu_{\text{air}}$
Re_{s_m}	=	Reynolds number based on transition region mean position $u_e \cdot s_m/\nu_{\text{air}}$
R_t	=	thermal resistance, K/W
Re_{Δ_2}	=	Reynolds number based on enthalpy thickness $u_e \cdot \Delta_2/\nu_{\text{air}}$
Re_{δ_2}	=	Reynolds number based on momentum thickness $u_e \cdot \delta_2/\nu$
Re_∞	=	Reynolds number based on airfoil chord and freestream velocity $V_\infty \cdot c/\nu_{\text{air}}$
Re_σ	=	Reynolds number based on transition region extension standard deviation $u_e \cdot \sigma/\nu_{\text{air}}$
r	=	high-speed aerodynamic recovery factor
St	=	gaseous flow local Stanton number $h_{\text{air}}/(\rho_{\text{air}} \cdot u_e \cdot c_{p,\text{air}})$
s	=	streamwise distance over airfoil surface, m
T	=	temperature, K
T_{tot}	=	total temperature, °C
U	=	overall heat transfer coefficient, W/(m^2 · K)
u	=	boundary layer streamwise velocity, m/s
V	=	velocity, m/s
v	=	boundary layer normal velocity, m/s
v_f	=	liquid water film velocity, m/s
$\bar{v}_f$	=	liquid water film mean velocity, m/s
y	=	distance normal to airfoil surface, m
α	=	angle of attack
β	=	local collection efficiency
Δs	=	finite volume length in streamwise direction, m
ΔT	=	temperature difference between gaseous flow interface and external flow, K
Δ_2	=	boundary layer enthalpy thickness, m
δ_f	=	liquid water film height, m
δ_1	=	boundary layer displacement thickness, m
δ_2	=	boundary layer momentum thickness, m
γ	=	probability of occurrence of turbulent flow regime
λ	=	pressure gradient parameter
μ	=	dynamic viscosity, Pa · s
ν	=	kinematic viscosity, m^2/s
ρ	=	density, kg/m^3
σ	=	transition region extension standard deviation, m
τ	=	shear stress applied on liquid water film surface by gaseous flow, Pa
φ	=	angle between the droplet trajectory and airfoil surface normal at impact point

Received 3 May 2006; revision received 22 August 2006; accepted for publication 23 August 2006.

*Graduate Student, Mechanical Engineering Department, Escola Politécnica, Avenida Professor Mello Moraes, 223; also Thermal Analyst, Environmental Systems Engineering, Embraer, São José dos Campos, Brazil, Brigadeiro Faria Lima, 2170. AIAA Member.

†Associate Professor, Mechanical Engineering Department, Escola Politécnica, Avenida Professor Mello Moraes, 2231; also Dean, University Dean Office, Praça Mauá 1, Instituto Mauá de Tecnologia, São Caetano do Sul, Brazil.

‡Professor, Mechanical Engineering Department, Avenida Professor Mello Moraes, 2231.

Subscripts

air	=	gaseous flow
anti-ice	=	ice protection heating
d	=	supercooled water droplet
e	=	external edge of boundary layer
G	=	location at external gaseous flow
imp	=	water droplets impingiment
in	=	finite volume inlet
int	=	liquid gas, if wet, or solid-gas interface, if dry
lam	=	laminar regime
lv	=	liquid-vapor saturation
m	=	transition region mean position
out	=	finite volume outlet
rec	=	recovery
ref	=	reference for water properties T = 273.15 K
S	=	location just above liquid water film
stag	=	airfoil leading edge stagnation point
tr	=	transition onset
turb	=	turbulent regime
wall	=	airfoil solid surface
water	=	liquid or vapor water
∞	=	freestream, nondisturbed flow
0	=	boundary layer interface with airfoil solid surface $y = 0$

Superscript

*	=	indicates the blowing effect in gaseous flow local Stanton number

I. Introduction

THE ice accretion on aircraft wings and stabilizers may cause some aerodynamic performance degradation, weight increase, control, and maneuver abilities difficulties, that may lead to an operational safety margin reduction. When the aircraft is flying through a supercooled water droplets cloud, which is in a metastable thermodynamic equilibrium, the ice accretion on some aerodynamic surfaces will occur if they are not adequately protected. To protect the airfoils and guarantee safe flight in icing conditions, commercial and some military aircraft have ice protection systems, which can be classified in deice and anti-ice types. The deice system cyclically operates to remove the ice layer formed after some exposition period. When the system is not actuated, the ice builds up on the airfoil; when it is actuated, the system removes the ice from the airfoil. On the other hand, the anti-ice system prevents any ice accretion on airfoils and continuously operates while the aircraft flies under icing conditions. Most commercial jetliners have thermal anti-ice systems that use either engine hot bleed air or electrical heaters. An electrothermal anti-ice system, for instance, consists of a set of electrical heaters installed spanwise and streamwise on the airfoil, mainly at regions exposed to droplets impingement. Basically, the anti-ice systems can operate in three regimes: 1) fully evaporative: the impinging water droplets are vaporized close to the impingement region; 2) evaporative: the runback water flows over the airfoil leading edge and evaporates in a position upstream to the end of protected area; and 3) running wet: water runback flows downstream the end of the protected area. Consequently, in the running wet regime, if the runback water flows to regions downstream the thermally protected zone, the water will freeze and form runback ice. Therefore, depending on height, shape, and roughness of residual ice, a significant degradation of the airfoil aerodynamic characteristics and aircraft operational performance may occur. An adequate thermal anti-ice numerical code shall be used for conception, integrated optimization of aircraft systems, architecture definition, ice protection system sizing, and system development. In addition, during the certification phase, the code shall support critical cases matrix definition and test campaign planning. As a result, if numerical results are validated, the icing tunnel and natural icing flight tests duration and costs can be minimized.

II. Previous Works

The classic icing codes LEWICE [1,2], TRAJICE2 [3,4], and ONERA2D [5] estimate ice shapes over nonprotected airfoil surfaces. A comprehensive review of the mathematical model and a comparison of these codes' prediction capabilities were published by Wright et al. [6]. The main modules of these classic icing codes are: 1) flowfield, which solves the flow around an airfoil; 2) droplets trajectories, which calculates droplets flow paths and the local collection efficiency; and 3) thermal balance, which estimates the ice growth and its two-dimensional shape by applying the first law of thermodynamics to water and adiabatic solid surface around the airfoil leading edge. The majority of anti-ice numerical codes use the first and second modules but replace the third one by another that considers anti-ice heat flux distribution to calculate surface temperatures and runback mass flow rate.

At British Royal Aircraft Establishment, Cansdale, and Gent [3] implemented one of the pioneering works regarding thermal balance around nonheated airfoils under icing conditions by extending Messinger's [7] mathematical model to compressible flow and water vapor local concentration. Gent [4] implemented the numerical code TRAJICE2, which predicts two-dimensional ice shapes on airfoils. The author approximated the flow over the airfoil leading edge as one over the frontal part of a cylinder and, by scaling experimental results of heat transfer around rough cylinders, developed an empirical expression to evaluate convection heat transfer coefficient on airfoil surfaces. Alternatively, Gent [4] implemented a boundary layer integral analysis to evaluate the laminar and turbulent heat transfer coefficient over a near isothermal without mass transfer effects. The laminar to turbulent transition is assumed to occur when critical Reynolds number based on roughness height is 600. As other classic icing codes, the heat transfer prediction is only valid for thin ice accretions, i.e., at the beginning of accretion process, in the absence of flow separation [8]. Gent et al. [9] developed a rotorcraft airfoil deicing code that evaluates heat transfer coefficient distribution with the same procedure adopted in TRAJICE2, however, the authors concluded that the evaluation of the convective heat transfer coefficient during deicing operations shall be improved in future researches.

Makkonnen [10] proposed a calculation procedure for laminar, transitional, and turbulent heat transfer between an air stream with droplets and a rough surface of an iced cylinder. The author used the heat transfer coefficient to predict icing in wires of electrical power transmission lines. The heat transfer coefficient around the cylinder surface is evaluated with the boundary layer integral analysis based on Kays and Crawford [11]. He implemented a laminar boundary layer conduction thickness evaluation with Smith and Spalding's [12] model and a turbulent Stanton number expression, which requires evaluation from boundary layer analysis and such as estimated experimentally by Pimenta et al. [13]. Both laminar and turbulent convective heat transfer coefficients are evaluated by analogy between momentum and heat transfer that assumes flow over a near isothermal surface without mass transfer. Additionally, Makkonnen [10] assumed an abrupt laminar to turbulent flow transition and that the momentum thickness has no discontinuity at transition point, i.e., $\delta_{2,\mathrm{lam}} = \delta_{2,\mathrm{turb}}$. The author also proposed a transition criteria based on an expression that correlates pressure gradient and roughness height effects to momentum boundary layer flow stability.

Wade [14], and Downs and James [15] developed a numerical code to simulate a hot air engine inlet anti-ice system. The authors used semi-empirical correlations to calculate the convection heat transfer coefficients at two regions of engine inlet: 1) between the impingent hot air jets, from piccolo tube, and the concave internal surface of the nacelle lip leading edge; 2) between the free stream flow, loaded with supercooled water droplets, and the exposed surface of the nacelle leading edge. In the latter, the authors modeled the external flowfield as a combination of a flow around the frontal part of a cylinder and a flow along two parallel flat plates. Therefore, the cylinder and flat plate correlations were forced to match to decrease deviation between numerical results and test data. To

improve the convective heat transfer evaluation and obtain solid surface temperature results closer to test data, Riley [16] used a CFD numerical tool to solve the flowfield and estimate the heat transfer on nacelle lip external surfaces exposed to droplets impingement and on internal surfaces subjected to engine bleed air heating. The author compared the thermal operational performance of several nacelle lip geometries as well as different configurations of blowing, circulating, and exhausting hot air in leading edge internal compartments.

Henry [17] developed a numerical code to predict parameters of deicing systems operation. The author modified ONERA2D [5] by introducing a different thermal balance procedure for deicing simulation. In a later work, Henry [18] applied a finite difference boundary layer solver to evaluate laminar and turbulent heat transfer coefficients over the airfoil nonisothermal surface coupled with a transient two-dimensional water freezing front based on an enthalpy method [19].

Al-Khalil [20] developed the mathematical model, which considers rivulets effects on thermal balance, and Al-Khalil et al. [21] implemented the numerical code ANTICE to predict parameters of a thermal anti-ice system operation. This code uses the flow solver as well as the droplets trajectory and boundary layer calculation routines from LEWICE code [22,23]. The standard thermal module of the LEWICE adopts Messinger [7] equations for the freezing process over an adiabatic airfoil surface. Al-Khalil et al. [21] extended the standard thermal balance for ice shape prediction to simulate anti-ice operation by considering airfoil surface heat flux distribution and a complete runback model with liquid water film breakdown into rivulets. Nevertheless, Al-Khalil et al. [21] used the same LEWICE boundary layer integral analysis in ANTICE code, despite it being dedicated to evaluating heat transfer over icing surfaces that are rough and near isothermal. Because of significant deviations between numerical results and experimental data for solid surface temperatures, the authors also implemented in the code the possibility to use directly the experimental heat transfer coefficient. For convection heat transfer calculation, this code estimates the laminar boundary layer conduction thickness, assumes a transition criteria triggered by roughness, and estimates turbulent heat transfer coefficient over a rough surface with similar assumptions and procedures adopted by Makkonnen [10].

Morency et al. [24] implemented a numerical code for anti-ice simulation and validated its results with experimental data from Al-Khalil et al. [21]. The authors published results of two versions of the main code: 1) CANICE A, which uses an experimental overall heat transfer coefficient; and 2) CANICE B, which uses an estimated by momentum and heat transfer analogy [11], a transition position arbitrarily imposed or estimated by Michel's classic correlation [25], and for fully the turbulent boundary layer, uses the turbulent expression developed by Ambrok [26]. Specifically, the CANICE B code considers some effects of streamwise airfoil surface temperature gradients when performing the thermal turbulent boundary layer integral analysis. Neither the model of laminar to turbulent flow transition nor the procedure to define the turbulent boundary layer virtual origin was described by the authors. Morency et al. [27] published the results of CANICE FD that uses a finite difference numerical scheme to calculate momentum, heat, and mass transfer in the flow around the airfoil. The procedure adopted takes into account the laminar and turbulent boundary layer as well as the transition region. Furthermore, it uses the Cebeci–Smith mixing length turbulence model for eddy viscosity that includes an intermittency function for the transition between laminar and turbulent flow regimes [25].

Silva and Silvares [28] described the development of the thermal anti-ice mathematical model in detail and summarized Silva's thesis bibliography research, results, conclusions, and contributions [29]. Silva et al. [30,31] briefly described the mathematical model, presented some numerical code results, and compared with experimental data and other codes' results for an anti-ice system operating in both evaporative and running wet regimes. Their mathematical model for anti-ice system simulation, which is detailed and analyzed described herein, applies the first law of thermodynamics to liquid water flow and solid airfoil surface together with the conservation of mass and momentum to liquid water flow. At first stages of mathematical model development, Silva [29] tried to use the ONERA2D boundary layer evaluation procedure, which adopts the Makkonnen model [10], in his new thermodynamic solver but the heat transfer coefficient in the turbulent region was overestimated. Like other classic icing codes, ONERA2D evaluates the convection heat transfer over fully rough surfaces, which is applicable to an airfoil with ice formation but not with thermal ice protection. Also, this procedure [10] assumes abrupt laminar to turbulent transition triggered by roughness and neglects the effects of the temperature gradient distribution in streamwise direction, as well as the coupling between evaporation and thermal boundary layer growth. Therefore, Silva et al. [30,31] implemented a numerical code to evaluate the integral equations of momentum and thermal boundary layers considering a nonisothermal airfoil surface with evaporation in laminar, transition, and turbulent flow regimes.

III. Objective

A novel thermal solver, which includes a boundary layer mathematical model with coupled heat and mass transfer effects, was developed for anti-ice numerical simulation and an extensive validation process was realized. This work is an extension of previous developments of Silva et al. [30,31] and proposes a mathematical procedure for estimation of airfoil electrothermal anti-ice system operational parameters.

IV. Reference Cases

Reference cases are necessary to determine the scope of the mathematical modeling, define the set of assumptions, simplify the equations, and support further results validation. They also determine the validity range of the results. Therefore, the reference cases were chosen based on the existence of reliable and recognized experimental data in open literature.

Al-Khalil et al. [21] performed anti-icing experiments at the Icing Research Tunnel at NASA Glenn Research Center facilities, Cleveland, Ohio. The authors measured surface temperature and overall heat transfer coefficient to validate ANTICE numerical code results. Several cases were run at the icing tunnel using an electrically heated airfoil for anti-icing system operation. As shown in Fig. 1, the airfoil was a 1.828 m span by 0.914 m chord, NACA 0012 profile with electronically controlled heaters. Each heater element in the streamwise direction had one thermocouple, one thermoresistor sensor, and one heat flux gauge installed. There were two sets of electrical heaters placed side-by-side spanwise and each heater set had seven individually controlled heaters. The total protected area was 0.914 m spanwise (two heater sets of 0.457 m) by 0.197 m streamwise (upper and lower surfaces at the leading edge region).

From this large experimental data set [21], representative runs at running wet, fully, and partially evaporative regimes were chosen to serve as references. During these test runs, the total electrical power provided to each heater set varied from 0.96 to 2.2 kW, true air speeds (TAS) varied from $V_\infty = 44.4$ to 88.8 m/s, but angle of attack was kept constant at $\alpha = 0$ deg. The associated icing test conditions were $T_{\text{tot}} = -21.6°\text{C}$, LWC = 0.55–0.78 g/m^3, and MVD = 20 μm, where LWC is liquid water content and MVD is median volumetric diameter.

V. Anti-Ice Simulation Overview

The mathematical model proposed by Silva et al. [30,31] requires the following: 1) the solution of velocity and pressure fields around the airfoil; 2) the calculation of droplet trajectories; 3) the application of the first law of thermodynamics to the liquid water and airfoil solid surface, plus the conservation of mass and momentum to the liquid water flow over the airfoil; and 4) the calculation of the dynamic and thermal boundary layers to obtain the coupled heat and mass transfer over the airfoil solid surface and liquid water flow.

The flowfield around airfoil and local collection efficiency data was obtained from an external numerical code ONERA2D [5] icing

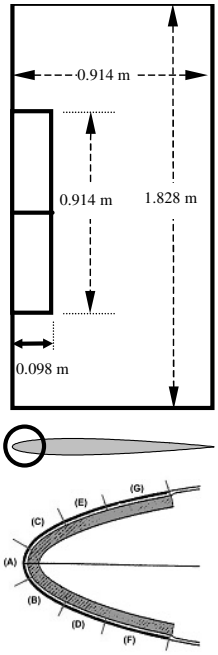

Fig. 1 Experimental model upper view and electrical heater distribution [5].

code but it can be also determined by other CFD tools. With this standard input data, the proposed mathematical model is able to predict operational parameters like solid surface temperatures, runback mass flow rate, and convection heat transfer coefficient distributions along the airfoil solid surface.

VI. Mathematical Model Description

Figure 2 shows the coordinates system and the five domains used in the present mathematical model, which are: 1) free stream flow, 2) gaseous flow, 3) momentum or thermal boundary layers, 4) water film flow, and 5) solid surface. By using this strategy for domain division, the mathematical model can be organized and simplified.

The first law of thermodynamics applied to solid surface (domain 5) results:

$$\frac{d}{ds}\left(k_{\text{wall}} \cdot \frac{dT_{\text{wall}}}{ds}\right) - F \cdot h_{\text{water}} \cdot (T_{\text{wall}} - T_{\text{water}}) + \dot{q}''_{\text{anti-ice}} + (1 - F) \cdot [-h_{\text{air}} \cdot (T_{\text{wall}} - T_{\text{rec}})] = 0 \tag{1}$$

Equation (1) considers conduction heat transfer in s direction but neglects in y direction. The heat flux distribution term $\dot{q}''_{\text{anti-ice}}$ in Eq. (1) is determined by electrical heater elements.

$$T_{\text{rec}} = (1 - r) \cdot T_e + r \cdot T_{\text{stag}} \tag{2}$$

$$T_e = T_{\text{stag}}/(1 + 0.2 \cdot M_e^2) \tag{3}$$

The recovery factor is assumed to be $Pr^{1/2}$ in laminar regime and $Pr^{1/3}$ in turbulent regime. A type of wetness factor is defined to represent the wetted area fraction in the finite volume ($F = 1$ if surface of liquid-gas interface is fully wet, $0 < F < 1$ if it is partially wet, $F = 0$ if it is fully dry). The last finite volume at the trailing edge on the upper or lower airfoil surface is considered to be adiabatic. The thermodynamic properties of air for high-speed flows can be evaluated at temperature [32]:

$$\bar{T}_{\text{air}} = T_e + 0.5 \cdot (T_{\text{int}} - T_e) + 0.22 \cdot (T_{\text{rec}} - T_e) \tag{4}$$

where solid-gas or liquid-gas interface temperature can assume the value of T_{wall} or T_{water}, if the airfoil surface is dry or wet, respectively.

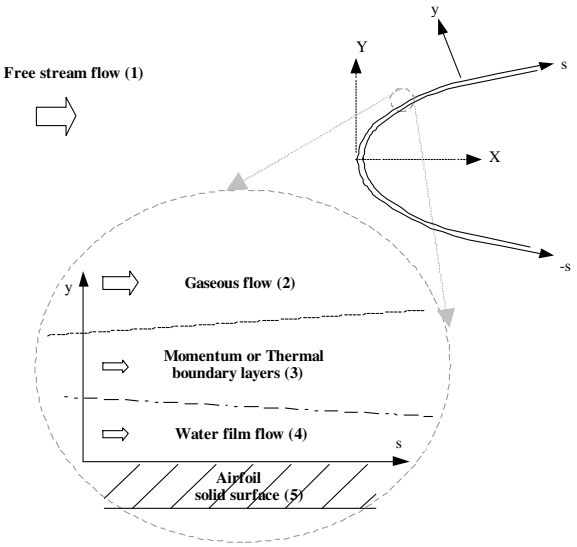

Fig. 2 Domains of the mathematical model.

By applying the first law of thermodynamics to the water film flow (domain 4), it is possible to obtain the following equation:

$$F \cdot A \cdot h^*_{\text{air}} \cdot (T_{\text{rec}} - T_{\text{water}}) + F \cdot A \cdot h_{\text{water}} \cdot (T_{\text{wall}} - T_{\text{water}}) + \dot{m}_{\text{in}} \cdot c_{p,\text{water}} \cdot (T_{\text{in}} - T_{\text{ref}}) - \dot{m}_{\text{out}} \cdot c_{p,\text{water}} \cdot (T_{\text{out}} - T_{\text{ref}}) + \dot{m}_{\text{imp}} \cdot \left[c_{p,\text{water}} \cdot (T_d - T_{\text{ref}}) + \frac{V_d^2}{2}\right] + \dot{m}_{\text{evap}} \cdot [i_{\text{lv}} - c_{p,\text{water}} \cdot (T_{\text{out}} - T_{\text{ref}})] = 0 \tag{5}$$

with

$$T_{\text{water}} = (T_{\text{in}} - T_{\text{out}})/2 \tag{6}$$

The convection heat transfer coefficient, between water film (4) and solid surface (5), is calculated by the Colburn analogy between momentum and heat transfer:

$$h_{\text{water}} = \rho_{\text{water}} \cdot v_f(s, \delta_f) \cdot c_{p,\text{water}} \cdot 0.5 \cdot C_f \cdot Pr_{\text{water}}^{-2/3} \tag{7}$$

The water thermodynamics properties are evaluated for low speed flows according to Eckert [32] at temperature

$$\bar{T}_{\text{water}} = T_{\text{wall}} + 0.5 \cdot (T_{\text{water}} - T_{\text{wall}}) \tag{8}$$

By applying the mass conservation principle to the water film flow (mathematical domain 4), the following equation is obtained:

$$\dot{m}_{\text{in}} + \dot{m}_{\text{imp}} = \dot{m}_{\text{out}} + \dot{m}_{\text{evap}} \tag{9}$$

According to Spalding [33], the water evaporation mass flux is calculated by

$$\dot{m}''_{\text{evap}} = g_m \cdot \text{B}_m \tag{10}$$

$$g_m = St \cdot G \cdot Le^{2/3} \cdot \frac{\ell_n(1 + B_m)}{B_m} \tag{11}$$

where B_m is calculated by the following expressions [11]:

$$B_m = \frac{mf_{\text{H2O},S} - mf_{\text{H2O},G}}{mf_{\text{H2O},S} - 1} \tag{12}$$

$$mf_{\text{H2O},G} = \frac{p_{\text{vap},G}}{1.61 \cdot p_{\text{mixt},G} - 0.61 \cdot p_{\text{vap},G}} \tag{13}$$

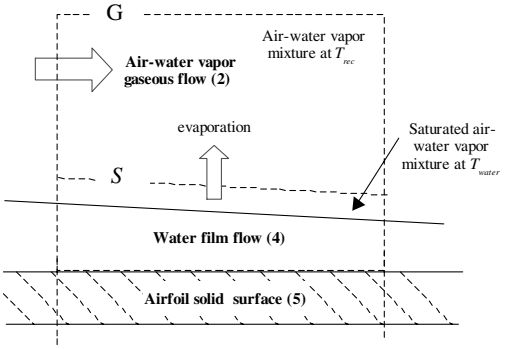

Fig. 3 Convective mass transfer model applied to anti-ice simulation.

$$mf_{\mathrm{H2O},S} = \frac{p_{\mathrm{vap},S}}{1.61 \cdot p_{\mathrm{mixt},S} - 0.61 \cdot p_{\mathrm{vap},S}} \tag{14}$$

Figure 3 presents the convective mass transfer model parameters and defines the location for evaluation of water vapor partial pressures: S, just above the liquid water film surface and G, at gaseous flow around the airfoil.

The heat transfer driving force is defined as [11,13,33]

$$B_h = \frac{\dot{m}''_{\mathrm{evap}}}{St^* \cdot G} \tag{15}$$

For the mass transfer, surface roughness, and pressure gradient levels of the reference cases defined herein, the effect of blowing on convective heat transfer is accounted for through

$$\frac{St^*}{St} = \frac{\ell_n(1 + B_h)}{B_h} \tag{16}$$

This is a coupled heat and mass transfer process where St^* depends on B_h, Eq. (16), that depends on both $\dot{m}''_{\mathrm{evap}}$ and St^*, Eq. (15). The iterative calculation process only finishes when the first law of thermodynamics, Eq. (5), is satisfied in each finite volume.

From the water droplet local collection efficiency definition, the impinging water flow is given by

$$\dot{m}_{\mathrm{imp}} = V_\infty \cdot \beta \cdot \mathrm{LWC} \cdot \Delta s \cdot 1 \tag{17}$$

At stagnation point, it is assumed that no runback water enters in the finite volume and Eq. (9) is solved from the stagnation point to the downstream direction for both lower and upper airfoil surfaces.

At the finite volume where T_{water} reaches solidification temperature, it was assumed that there is no outlet runback water mass flow rate, $\dot{m}_{\mathrm{out}} = 0$, which denotes the beginning of the water freezing. Neither the effects of solidification enthalpy is considered in Eq. (5) nor the existence of partially frozen water runback is included in Eq. (9). These are crude assumptions to forecast the water freezing location and ice growth, however, they are conservative enough to inform if the system is not performing adequately. In addition, one of the objectives of the present work is to predict performance of an anti-ice system, which is designed to prevent ice formation and operate at higher average temperatures than 0°C. If the warming effect due to enthalpy releasing had been considered, the model would have indicated the water freezing initiation in a further position than predicted by this model. Al-Khalil [20] used similar conservative assumptions for the freezing process in his basic model.

To compare the numerical results of present work with experimental data [21], an overall heat transfer coefficient was defined, taking into account the effects of convective heat transfer rate across solid-liquid and liquid-gas surface interfaces (i.e., h_{water} and h_{air}), runback water enthalpy net flux, water droplets impingement enthalpy, and evaporation enthalpy:

$$U = \frac{\dot{q}_{\mathrm{lost}}}{1 \cdot \Delta s \cdot \Delta T} \tag{18}$$

$$\dot{q}_{\mathrm{lost}} = R_t^{-1} \cdot 1 \cdot \Delta s \cdot \Delta T - \dot{m}_{\mathrm{evap}} \cdot (i_{\mathrm{lv}} + i_{\mathrm{water}}) + \dot{m}_{\mathrm{imp}} \cdot i_d + \dot{m}_{\mathrm{in}} \cdot i_{\mathrm{in}} - \dot{m}_{\mathrm{out}} \cdot i_{\mathrm{out}} \tag{19}$$

The momentum conservation equation for the water film in the present case is

$$\frac{1}{\rho_{\mathrm{water}}} \cdot \frac{\partial p_e}{\partial s} = \nu_{\mathrm{water}} \cdot \frac{\partial^2 v_f(s,y)}{\partial y^2} \tag{20}$$

Equation (20) is solved by applying the boundary conditions at the water film flow (4):

$$y = \delta_f \Rightarrow \mu_{\mathrm{water}} \cdot \left[\frac{\partial v_f(s,y)}{\partial y}\right]_{\delta_f} = \tau + \dot{m}''_{\mathrm{imp}} \cdot V_d \cdot \sin\varphi \qquad y = 0 \Rightarrow v(s,y) = 0 \tag{21}$$

The velocity profile of the water film, after the solution of Eq. (20), is

$$v_f(s,y) = \frac{\partial p_e}{\partial s} \cdot \frac{y^2}{2 \cdot \mu_{\mathrm{water}}} + \left[\tau + \dot{m}''_{\mathrm{imp}} \cdot V_d \cdot \sin\varphi - \delta_f(s) \cdot \frac{\partial p_e}{\partial s}\right] \cdot \frac{y}{\mu_{\mathrm{water}}} \tag{22}$$

The water film thickness can be calculated from the mean water film velocity, which is obtained with Eq. (22), and is given by

$$\delta_f = \frac{\dot{m}_{\mathrm{in}} + \dot{m}_{\mathrm{out}}}{2 \cdot \rho_{\mathrm{water}} \cdot \bar{v}_f} \tag{23}$$

VII. Gaseous Flow Boundary Layers

The evaluation of the convective heat transfer and friction coefficients distribution around the airfoil is performed by solving the thermal and dynamic boundary layers equations in integral form at laminar and turbulent regimes. For laminar-turbulent transition regime, it is proposed a linear combination of turbulent and laminar results weighted by an exponential probability function.

In the present paper, both momentum and thermal boundary layer equations are simplified considering a steady-state and one-dimensional flow with moderate pressure gradient over a smooth, nonisothermal, and impermeable surface. These assumptions lead to Eqs. (24) and (31). Note that evaporation mass flux is neglected in those equations, however, the effect of blowing in convective heat transfer is estimated, Eqs. (15) and (16), during calculation of water liquid film and airfoil solid surface temperatures. The solution of thermal boundary layer equation provides the value of St with no blowing to estimate $\dot{m}''_{\mathrm{evap}}$ and B_h so that the St^* with blowing effect is calculated.

The boundary layer momentum equation can be conveniently expressed in a nondimensional equation of momentum thickness [11]:

$$\frac{C_f}{2} = \frac{d\delta_2}{ds} + \delta_2 \cdot \left[\left(2 + \frac{\delta_1}{\delta_2}\right) \cdot \frac{1}{u_e} \cdot \frac{du_e}{ds}\right] \tag{24}$$

Based on Thwaites' [34] approximation, Kays and Crawford [11] integrated Eq. (24) to obtain the momentum thickness in laminar flow regime:

$$\delta_{2,\mathrm{lam}} = \frac{0.664 \cdot \nu_{\mathrm{air}}^{1/2}}{u_e^{2.84}} \cdot \left(\int_{s_{\mathrm{stag}}}^{s_{\mathrm{tr}}} u_e^{4.68}\, \mathrm{d}s\right)^{1/2} \tag{25}$$

The laminar friction coefficient $C_{f,\mathrm{lam}}$ is evaluated in a function of the pressure gradient parameter by the procedure developed by Cebeci and Bradshaw [25]:

$$C_{f,\mathrm{lam}} = \frac{2 \cdot l(\lambda)}{Re_{\delta_2}} \tag{26}$$

where

$$l(\lambda) = \begin{cases} 0.225 + 1.61 \cdot \lambda - 3.75 \cdot \lambda^2 + 5.24 \cdot \lambda^3 & 0 < \lambda < 0.1 \\ 0.225 + 1.472 \cdot \lambda - (0.0147 \cdot \lambda)/(\lambda + 0.107) & 0 > \lambda > -0.1 \end{cases} \tag{27}$$

For the present work, the integral equation of momentum thickness in turbulent regime, Eq. (24), is satisfactorily simplified to [11]

$$\delta_{2,\text{turb}} = \frac{0.036 \cdot \nu_{\text{air}}^{1/5}}{u_e^{3.29}} \cdot \left(\int_{s_{\text{tr}}}^{s} u_e^{3.86} \, \text{d}s \right)^{0.8} + \delta_{2,\text{tr}} \tag{28}$$

Equation (28) is evaluated with $\delta_{2,\text{tr}} = \delta_{2,\text{lam}} = \delta_{2,\text{turb}}$, i.e., Eq. (25) provides the initial condition for the integral in Eq. (28) at transition onset position s_{tr}. With momentum thickness, $Re\delta_{2,\text{turb}}$ is obtained to allow evaluation of turbulent local friction coefficient by

$$\frac{C_{f,\text{turb}}}{2} = 0.0125 \cdot Re_{\delta_{2,\text{turb}}}^{-0.25} \tag{29}$$

At airfoil stagnation point, the local convective heat transfer is approximated by [12]

$$Nu_{\text{stag}} = \left[0.246 \cdot Re_{\infty} \cdot \frac{d(u_e/V_{\infty})}{d(s/c)} \bigg|_{s=s_{\text{stag}}} \right]^{1/2} \tag{30}$$

To evaluate the local convective heat transfer coefficient distribution downstream of the stagnation point in upper and lower airfoil surfaces, it is convenient to represent the thermal boundary layer as [11]

$$St = \frac{d\Delta_2}{ds} + \Delta_2 \cdot \left(\frac{1}{u_e} \cdot \frac{du_e}{ds} + \frac{1}{i_0} \cdot \frac{di_0}{ds} \right) \tag{31}$$

From Eq. (31), Ambrok [26] developed an original expression to evaluate laminar local convective heat transfer due to a flow over nonisothermal surfaces with moderate pressure gradient:

$$Nu_{\text{lam}} = 0.3 \cdot Re_s \cdot \Delta T \cdot \left(\int_{s_{\text{stag}}}^{s_{\text{str}}} \frac{u_e \cdot \Delta T^2}{\nu_{\text{air}}} \, \text{d}s \right)^{-1/2} \tag{32}$$

The evaluation of $\Delta_{2,\text{turb}}$ by Eq. (35) requires the knowledge of the $\Delta_{2,\text{lam}}$ value at onset transition location as initial condition. Thus, Eq. (31) is simplified to give the following expression [26]:

$$Re_{\Delta_{2,\text{lam}}} = \frac{0.83}{\Delta T} \cdot \left(\int_{s_{\text{stag}}}^{s_{\text{tr}}} \frac{u_e \cdot \Delta T^2}{\nu_{\text{air}}} \, \text{d}s \right)^{1/2} \tag{33}$$

The local convective heat transfer in turbulent regime is evaluated by [11,26]

$$St_{\text{turb}} = 0.0125 \cdot Re_{\Delta_{2,\text{turb}}}^{-0.25} \cdot Pr^{1/2} \tag{34}$$

Like the momentum boundary layer analysis, it is assumed that enthalpy thickness is a continuous function at the beginning of the transition region location. Therefore, with the value of Eq. (33) at transition onset and assumption of $\Delta_{2,\text{tr}} = \Delta_{2,\text{lam}} = \Delta_{2,\text{turb}}$, the turbulent enthalpy thickness is approximately evaluated by

$$Re_{\Delta_{2,\text{turb}}} \cdot \Delta T = \left[0.0156 \cdot Pr^{-1/2} \cdot \mu_{\text{air}}^{-1} \cdot \int_{s_{\text{tr}}}^{s} G \cdot \Delta T^{1.25} \, \text{d}s + (Re_{\Delta_{2,\text{tr}}} \cdot \Delta T_{\text{tr}})^{1.25} \right]^{0.8} \tag{35}$$

VIII. Laminar-Turbulent Transition in Gaseous Flow

Sogin [35] found that an adequate convection heat transfer calculation around an airfoil equipped with an ice protection system requires the knowledge of the laminar-turbulent transition position. The same author observed that a finite transition region extension occurs under icing conditions and that it may be longer in icing tunnel tests than in natural icing flights.

Usually, the classic icing codes assume that transition occurs abruptly in a position s_{tr}. Based on literature and experimental evidence, it is proposed in the present model to represent the transition as a region with defined length where the flow goes from fully laminar to fully turbulent regime.

Reynolds et al. [36] defined the laminar-turbulent transition region statistically by a mean position and a standard deviation length. The authors defined a normal cumulative distribution, which goes from zero at lower Re_s limits (fully laminar) to unity at upper Re_s limits (fully turbulent). This function describes the probability of the turbulent flow regime to appear at a certain position upstream to s. Both St and C_f within the transition region are calculated by a linear combination of the laminar $C_{f,\text{lam}}$ and St_{lam} with turbulent $C_{f,\text{turb}}$ and St_{turb} values. The transition model adopted herein [36] was developed based on the experiments performed by Schubauer and Klebanoff [37].

The heat transfer flux from the interface surface (solid-gas or liquid-gas) to gaseous flow is approximately represented by

$$\dot{q}''(s) = [1 - \gamma(s)] \cdot \dot{q}''_{\text{lam}}(s) + \gamma(s) \cdot \dot{\bar{q}}''_{\text{turb}}(s) \tag{36}$$

where γ is the probability of turbulent flow to occur upstream s position.

Equation (36) can be expressed in a more convenient nondimensional form as

$$St(s) = \begin{cases} St_{\text{lam}}(Re_s) & s < s_m - 2 \cdot \sigma \\ [1 - \gamma(s)] \cdot St_{\text{lam}}(Re_s) + \gamma(s) \cdot St_{\text{turb}}(Re_s) & s \geq s_m - 2 \cdot \sigma \end{cases} \tag{37}$$

where s_m is the mean position where $\gamma = 50\%$, and $s_m - 2 \cdot \sigma$ is the position where $\gamma < 3\%$. The Reynolds numbers used to define the transition region are Re_s, Re_{s_m} and Re_σ. Similarly, the linear combination procedure is also applied to friction coefficient calculation C_f, i.e., the $St(s)$ is replaced by $C_f(s)$ in Eq. (37).

The turbulent flow probability $\gamma(Re_s)$ is evaluated by

$$\gamma(Re_s) = \int_{-\infty}^{Re_s} \left(\frac{1}{Re_s \cdot \sqrt{2 \cdot \pi}} \right) \cdot \exp\left[\frac{-(Re_s - Re_{s_m})^2}{(2 \cdot Re_\sigma^2)} \right] \text{d}(Re_s) \tag{38}$$

For ice protection systems simulation, the values of s_m and σ from Eq. (37) are usually defined from either experimental data or previous experience. It is recommended to be attentive when using classical semi-empirical criteria, such as the one developed by Michel [25], or automated procedures to predict the onset and length of the transition region. These procedures may have a limited validity range and, therefore, not be applicable to predict transition parameters of flows around heated airfoils under natural ice flights or icing tunnel conditions.

IX. Conclusions

The present paper proposes an innovative procedure to evaluate heat and mass transfer over dry and wet surface regions of an airfoil containing an electrothermal ice protection system. Although laminar, transition, and turbulent boundary layer models have been used in other applications, such as gas turbine vane cooling, this approach is not applied to the airfoil anti-ice numerical simulation. The coupled mass transfer model used in the present work has been similarly applied to paper drying process simulation and condenser designs, however, they have limited or no application to aircraft ice protection in the reviewed bibliography.

To decrease the deviations between model predictions and experimental data for airfoil surface temperature distribution,

previous authors adopted finite difference, finite volume schemes, or even CFD commercial tools because they did not have satisfactory results when using conventional boundary layer integral analysis. The classic icing codes evaluate the heat transfer coefficient with momentum boundary layer parameters and roughness height by using one of momentum and heat transfer analogies. In other mathematical models, the authors adopted even more limited semi-empirical expressions for convection heat transfer estimation. As a result, some of the procedures proposed by previous researchers are likely to be more adequate for estimation of the heat and mass transfer around nonheated airfoils with rough and near isothermal icing surfaces. The present model proposes a boundary layer integral analysis to estimate the coupled heat and mass transfer over heated airfoils with nonisothermal and relatively smooth surfaces, which is the case of an airfoil equipped with anti-ice systems.

In addition, most previous works considered an abrupt laminar to turbulent flow transition. The present work, on the other hand, proposes a continuous and smooth transition region mathematical model to link the laminar to turbulent flow regimes. This transition region estimation procedure is applied to both momentum and thermal boundary layer parameters. Some evidence has indicated the adequacy of the present transition region model such as experimental data and previous researchers' observations. Furthermore, it is clear that some finite difference codes succeeded in estimating convective heat transfer within a laminar-turbulent transition region due to the incorporation of an intermittency function in their turbulence models.

In sum, the present paper contributes to a more satisfactory estimation of heat and mass transfer around an ice-protected airfoil because it considers the following: 1) an evaporation model based on convective mass transfer; 2) a coupling between convection heat transfer coefficient and solid-gas or liquid-gas interface temperatures due to evaporation mass flux effects in thermal boundary layer; 3) a solution of laminar and turbulent thermal boundary layer around the airfoil considering a flow with variable properties and moderate pressure gradient over a smooth surface with streamwise temperature gradient; 4) a model considering a smooth transition from laminar to turbulent flow in a finite region; and 5) a continuity condition at the laminar to turbulent transition onset position, where the initial condition for turbulent enthalpy and momentum thicknesses calculation correspond to the respective laminar values at same position.

Acknowledgments

The authors would like to acknowledge Marcos de Mattos Pimenta for his contributions in laminar to turbulent transition subject and boundary layer modeling aspects. Guilherme A. L. da Silva thanks Brazilian jet aircraft manufacturer, Embraer and Roberto Petrucci, Environmental Systems Engineering Manager, for all the support that allowed the publishing of this work.

References

[1] Macarthur, C., Keller, J., and Luers, J., "Mathematical Modeling of Airfoil Ice Accretion on Airfoils," AIAA Paper 82-36042, 1982.

[2] Ruff, G. A., and Berkowitz, B. M., Users Manual for the NASA Lewis Ice Accretion Prediction Code (LEWICE), NASA CR-185129, 1990.

[3] Cansdale, J. T., and Gent, R., "Ice Accretion on Aerofoils in Two-Dimensional Compressible Flow: A Theoretical Model," Royal Aircraft Establishment RAE TR 82128, Farnborough, UK, 1983.

[4] Gent, R., "TRAJICE2: A Combined Water Droplet Trajectory and Ice Accretion Prediction Program for Aerofoils," Royal Aircraft Establishment RAE TR 90054, Farnborough, UK, 1990.

[5] Guffond, D., and Brunet, L., "Validation du Programme Bidimensionnel de Capitation," ONERA Rapport Technique RP 20/5146 SY, Châtillon Cedex, France, 1988.

[6] Wright, W., Gent, R., and Guffond, D., "DRA/NASA/ONERA Collaboration on Icing Research Part 2: Prediction of Airfoil Ice Accretion," NASA CR 202349, Cleveland, OH, May 1997.

[7] Messinger, B. L., "Equilibrium Temperature of an Unheated Icing Surface as a Function of Air Speed," *Journal of the Aeronautical Sciences*, Vol. 20, No. 1, 1953, pp. 29–42.

[8] Gent, R. W., Dart, N. P., and Cansdale, J. T., "Aircraft Icing," *Philosophical Transactions of the Royal Society of London, Series A: Mathematical and Physical Sciences*, Vol. 358, No. 1776, 2000, pp. 2873–2911.

[9] Gent, R. W., Moser, R., Cansdale, J. T., and Dart, N. P., "Role of Analysis in the Development of Rotor Ice Protection System," Society of Automotive Engineers Paper 2003-01-2090, 2003.

[10] Makkonnen, L., "Heat Transfer and Icing of a Rough Cylinder," *Cold Regions Science and Technology*, Vol. 10, No. 2, 1985, pp. 105–116.

[11] Kays, W. M., and Crawford, M. E., *Convective Heat and Mass Transfer*, McGraw–Hill, New York, 1993.

[12] Smith, A. G., and Spalding, D. B., "Heat Transfer in a Laminar Boundary Layer with Constant Fluid Properties and Constant Wall Temperature," *Journal of the Royal Aeronautical Society*, Vol. 62, Jan. 1958, pp. 60–64.

[13] Pimenta, M. M., Moffat, R., and Kays, W. M., "Turbulent Boundary Layer: An Experimental Study of the Transport of Momentum and Heat with the Effects of Roughness," Stanford Univ. Report HMT-21, Thermosciences Division, Mechanical Engineering Dept., Stanford, CA, May 1975.

[14] Wade, S. J., "Modeling of the Performance of a Thermal Anti-Icing System for use on Aero-Engine Intakes," M.S. Thesis, Loughborough Univ. of Technology, Loughborough, UK, 1986.

[15] Downs, S. J., and James, E. H., "Heat Transfer Characteristics of an Aero-Engine Intake Fitted with a Hot Air Jet Impingement Anti-Icing System," *Proceedings of 25th National Heat Transfer Conference*, Vol. 1, American Society of Mechanical Engineers, 1988, pp. 163–170.

[16] Riley, S. J., "Investigation Relating Factors Influencing the Effectiveness of an Aero-Engine Intake Thermal Anti-Icing System," Ph.D. Thesis, Loughborough Univ. of Technology, Loughborough, UK, 1991.

[17] Henry, R., "Etude du Fonctionnement d'Undegivreur Electrique: Modelisation et Mesure en Soufflerie Givrante de Temperature Parietale par Thermographie Infrarouge," Ph.D. Thesis, Blaise Pascal Univ., Clemont-Ferrand, France, 1989.

[18] Henry, R., "Development of an Electrothermal De-Icing/Anti-Icing Model," ONERA TAP 92005, Chatillon Cedex, France, 1992.

[19] Raw, M., and Schneider, G., "New Implicit Solution Procedure for Multidimensional Finite-Difference Modeling of the Stefan Problem," *Numerical Heat Transfer*, Vol. 8, No. 5, 1985, pp. 559–571.

[20] Al-Khalil, K. M., "Numerical Simulation of an Aircraft Anti-Icing System Incorporating a Rivulet Model for the Runback Water," Ph.D. Thesis, Univ. of Toledo, Toledo, OH, 1991.

[21] Al-Khalil, K. M., Horvath, C., Miller, D. R., and Wright, W., "Validation of NASA Thermal Ice Protection Computer Codes Part 3: Validation of ANTICE," NASA TM 2001-210907, Cleveland, OH, May 2001.

[22] Wright, W. B., "User Manual for the Improved NASA Lewis Ice Accretion Code LEWICE 1.6," NASA CR 198355, Cleveland, OH, May 1995.

[23] Wright, W. B., "User Manual for the NASA Glenn Ice Accretion Code LEWICE Ver. 2.0," NASA CR 209409, Cleveland, OH, 1999.

[24] Morency, F., Tezok, F., and Paraschivoiu, I., "Heat and Mass Transfer in the Case of an Anti-Icing System Modelization," AIAA Paper 99-0623, 1999.

[25] Cebeci, T., and Bradshaw, P., *Physical and Computational Aspects of Convective Heat Transfer*, Springer–Verlag, Berlin, 1984.

[26] Ambrok, G. S., "Approximate Solution of Equations for the Thermal Boundary Layer with Variations in Boundary Layer Structure," *Soviet Physics Technical Physics*, Vol. 2, No. 9, 1957, pp. 1979–1986.

[27] Morency, F., Tezok, F., and Paraschivoiu, I., "Anti-Icing System Simulation Using CANICE," *Journal of Aircraft*, Vol. 36, No. 6, 1999, pp. 999–1006.

[28] Silva, G. A. L., and Silvares, O. M., "Airfoil Anti-Ice System Thermal Simulation," Technical Bulletin BT / PME / 0207, Escola Politécnica da Univ. de São Paulo, São Paulo, Brazil, 2002.

[29] Silva, G. A. L., "Modelagem e Simulação da Operação de Sistema Antigelo Eletrotérmico de um Aerofólio," M.S. Thesis, Escola Politécnica da Univ. de São Paulo, São Paulo, Brazil, April 2002.

[30] Silva, G. A. L., Silvares, O. M., and Zerbini, E. J. G. J., "Airfoil Anti-Ice System Modeling and Simulation," AIAA Paper 2003-0734, 2003.

[31] Silva, G. A. L., Silvares, O. M., and Zerbini, E. J. G. J., "Simulation of an Airfoil Electro-Thermal Anti-Ice System Operating in Running Wet Regime," AIAA Paper 2005-1374, 2005.

[32] Eckert, E. R. G., "Engineering Relations for Friction and Heat Transfer to Surfaces in High Velocity Flow," *Journal of the Aeronautical Sciences*, Vol. 22, No. 8, Aug. 1955, pp. 585–587.

[33] Spalding, D. B., *Convective Mass Transfer, an Introduction*, McGraw–

Hill, New York, 1963.
[34] Thwaites, B., Approximate Calculation of the Laminar Boundary Layer, *Aeronautical Quarterly*, Vol. 1, 1949, pp. 245–280.
[35] Sogin, H. H., "Design Manual for Thermal Anti-Icing Systems," Technical Report Wright Air Development Division 54-313, IL, 1954.
[36] Reynolds, W. C., Kays, W. M., and Kline, S. J., "Heat Transfer in the Turbulent Incompressible Boundary Layer 4: Eeffect of Location of Transtion and Prediction of Heat Transfer in a Known Transition Region," NASA, Memo 12-4-58W, Washington, DC, Dec. 1958.
[37] Schubauer, G. B., and Klebanoff, P. S., "Contributions on the Mechanics of Boundary-Layer Transition," NACA, Report 1289, Washington, DC, 1955.